Korean J. of Chem. Eng., 12(4), 428-435 (1995)

A STOCHASTIC ANALYSIS OF CONTAMINANT TRANSPORT THROUGH A ROUGH-SURFACED FRACTURE

Chung-Kyun Park†, Dong-Kwon Keum and Pil-Soo Hahn

Nuclear Environment Management Center, Korea Atomic Energy Research Institute,
Daeduk Science Town P.O. Box 105, Taejon, Korea
(Received 3 December 1994 • accepted 17 May 1995)

Abstract—A stochastic model for the calculation of flow and contaminant transport in a single fracture with variable apertures was presented. The spatially varying apertures of the fracture were generated using a geostatistical method, based on a given aperture probability density distribution and a specified spatial correlation length. Fluid flowed between two points in the fracture plane. The fluid potential at each node of the discretization mesh was computed and the steady state flow rates between all the nodes were obtained. Then the contaminant transport was calculated using a particle tracking method. The migration plumes of contaminant between the inlet and the outlet were displayed in contour plots and contaminant elution profiles were also plotted. Calculations showed that fluid flow occured predominantly in a few preferred paths. Hence, the large range of apertures in the fracture gives rise to flow channeling. Simulation results were correlated with the basic input parameters: standard deviation of a lognormal aperture distribution function and the spatial correlation length.

Key words: *Contaminant Transport, Stochastic, Variable Aperture, Fracture, Particle Tracking*

INTRODUCTION

In recent years studies have been increased in the area of flow and transport of contaminants in underground. Many countries are considering siting or already running repositories for industrial toxic wastes including radioactive wastes. To assess whether a toxic species is sufficiently isolated from the biosphere, informations in several fields are needed. There is, however, less information and experience on underground environment, especially on deep hard rock environment. When toxic species are disposed of in underground hard rock, the species that are dissolved in groundwater will be carried away through the rock fracture by the flowing water in the long run. Some mathematical modeling works have been carried out to characterize such flow fields [Choi et al., 1988; Lee et al., 1990; Keum et al., 1994; Park et al., 1995].

Recent approaches to model flow in fractured medium can be classified into two groups; equivalent porous medium model [Tang et al., 1981] and discrete fracture model [Tsang and Tsang, 1987]. The porous medium model characterizes hydrodynamic parameters by averaged values and has been applied to the flow in soils. When the flow medium has extremely many interconnecting fractures, the flow medium can be treated as an equivalent porous medium. Otherwise, a discrete fracture model will be more appropriate. The flow in a fracture is often assumed to be like that between two parallel and smooth plates. However, results from field and laboratory measurements show that the parallel plate idealization of a rock fracture does not describe adequately the fluid flow and contaminant transport in a single fracture [Moreno et al., 1985; Moreno and Neretnieks, 1993]. The parallel plate model fails to recognize the spatial heterogeneity in the fracture aperture. Conceptual models of aperture heterogeneity have been studied by Neretnieks et al. [1982] and Moreno et al. [1988]. The contaminant was assumed to be advected along parallel flow paths of different aperture that did not intersect. Tsang et al. [1988] extended this conceptual model by assuming spatial variability in the fracture aperture along each flow path. Park et al. [1995] measured aperture distribution of a natural granite fracture of 1×1 m scale by a hydraulic test. They found that the aperture distributed in the order of 10^{-4} m. Tsang and Tsang [1987] indicated that the apertures follow a gamma distribution from the results of surface profiling measurements on 12 cm cores of a natural fracture in granite. Apparent apertures that have been observed in cores or well logs measured by Bianchi and Snow [1968] were found to follow a lognormal distribution.

Simulation techniques for multidimensional random fields have many applications in hydrology. There are several simulation techniques being developed: nearest-neighbor method [Smith and Schwartz, 1980], matrix decomposition method [Nash, 1979], spectral method [El-Kadi, 1984] and turning-band method [Mantoglou and Wilson, 1982]. The first two matrix models represent the field at a number of prespecified discrete points. Assuming stationarity, these models attempt to preserve the covariance of the field between these points. The matrix decomposition approach is used to decompose a symmetric, non-negative-definite matrix into a lower triangular matrix. Random fields can be characterized not only at the descrete points but also at every other point within the area of interest. The other two methods are developed for this purpose.

In the present work, we therefore present our investigations of flow in two-dimensions, corresponding to the physical situation of flow in a single fracture, taking into account the variable apertures in the plane of the fracture. By solving for the flow in two dimensional fracture, we attempt to understand the flow characteristics in the fracture and to identify the key parameters that control the channeling flow pattern.

†To whom all correspondences should be addressed.

FRACTURE APERTURE GENERATION

From the flow and transport viewpoint, a fracture is described by the aperture between the fracture surfaces. Since the fracture surfaces are rough and undulating the apertures vary spatially. The variation of the fracture aperture in the fracture plane may be characterized by a spatial correlation length and an aperture density distribution. This means that for distances in the fracture plane smaller than the correlation length the aperture values are more likely to be similar, but at distances larger than the correlation length there is little or no correlation between apertures at different locations. The fracture plane is partitioned by grids with a different aperture assigned to each square enclosed by grid lines. In the present study, the number of squares are 20 by 20. The assignment of the apertures is done by a geostatistical method which generates a two-dimensional field of a correlated distributed parameter [Moreno et al., 1988].

For the purpose of this study we chose a lognormal distribution for the variable apertures in the plane of the single fracture and an exponential function for the spatial covariance of the apertures to generate different aperture values in the fracture plane divided into square meshes. The martix decomposition method is used to generate the lognormally distributed values of fracture apertures b which are first transformed to the normal distribution Y

$$Y=\log_{10} b \tag{1}$$

The values of Y are estimated from

$$Y=M\varepsilon+\nu \tag{2}$$

in which ν is the mean of Y, ε is a vector N [0, 1], i.e., normally distributed with mean of zero and standard deviation of 1, and M is defined in terms of the covariant matrix:

$$A=M\ M^T \tag{3}$$

Eq. (2) represents the generated process because the mean is given by

$$E[Y]=M\ E[\varepsilon]+\nu=\nu \tag{4}$$

in which E[ ] stands for the expectation operator. The covariance is given by

$$E[(Y-\nu)(Y-\nu)^T]=M\ E[\varepsilon\varepsilon^T]\ M^T=M\ M^T=A \tag{5}$$

We use the exponential form of the covariance function [13]:

$$A=\sigma^2\ \exp\ (-\alpha r) \tag{6}$$

in which σ^2 is the variance of Y, r is the distance between adjacent two points, and α is the autocorrelation parameter which has the dimension of inverse length. The exponential form of Eq. (6) indicates that quantities within a distance on the order of $2/\alpha$ will be correlated and thus we may define the correlation length, λ, to be $2/\alpha$. The form of Eq. (6) indicates that the covariance chosen is isotropic. An anisotropic form of the covariance function may also be chosen. The generation scheme is performed as follows. First, the covariance matrix A is formed by using Eq. (6) for a set of different locations. Second, the matrix M is estimated using the Choleski decomposition technique. Third, the vector ε is generated from the distribution N[0, 1]. A set of vector ε is calculated by generating random numbers in computer subroutine. Hence, a different starting number or seed (R_n) gives a different set of vector ε. Finally, the vector Y is estimated from Eq. (2).

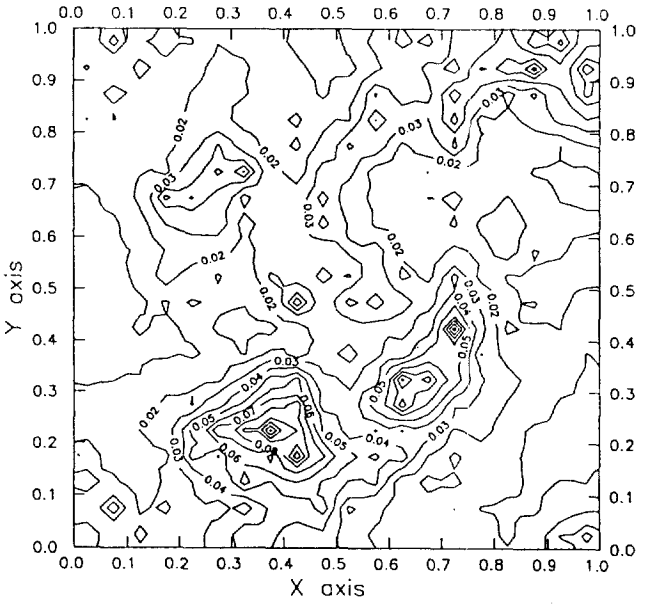

Fig. 1. Contour of aperture distribution in the rock surface of Test No. 1.
$\sigma=0.6$, $\lambda=0.5$, $R_n=1$

Table 1. Parameter values and simulation results

Set no.	Test no.	ν	R_n	σ	λ	t_m	σ_l^2	Pe
Set 1:	1	1	1	0.6	0.5	48	5.71	0.35
Different	6	1	2	0.6	0.5	56	1.75	1.14
Realization	7	1	3	0.6	0.5	60	3.17	0.63
Set 2:	4	1	1	0.1	0.5	25	0.77	2.6
σ	5	1	1	0.3	0.5	30	1.43	1.4
Variation	1	1	1	0.6	0.5	48	5.71	0.35
Set 3:	2	1	1	0.6	0.1	98	200	0.01
λ	3	1	1	0.6	0.25	60	11.1	0.18
Variation	1	1	1	0.6	0.5	48	5.71	0.35

Figs. 1 and 2 show seven realizations of statistically generated aperture field with identical mean of the lognormal aperture density distribution of $\nu=1.0$. The values of parameters are arranged in Table 1 for seven test cases. A grid of 20 by 20 nodes was used. Fig. 1 shows a contour plot of aperture distribution of Test No. 1: the mean $\nu=1$, the standard deviation $\sigma=0.6$, and the correlation length $\lambda=0.5$. The correlation length is expressed in terms of a fraction of the linear extent of the fracture plane. The numeric data in the contour map mean the values of apertures in the unit of cm. Fig. 2 shows surface plots of seven test cases. Here y axis are exaggerated for easy understanding. Figs. 2(a), 2(b) and 2(c) show λ variation from the value of 0.1 to 0.5. Figs. 2(a), 2(d) and 2(e) show σ variation from the value of 0.1 to 0.6. Figs. 2(a), 2(f) and 2(g) show different realization of the same density distribution function of Test No. 1 but with different initial numbers (R_n). The overall morphology of the fracture surface and flow paths are schemed to be roughly maintained with variation of λ and σ in this generating algorithm, while the morphology and flow paths are changed with the variation of R_n.

FLOW IN THE FRACTURE

The fluid flow through the fracture is then calculated for a

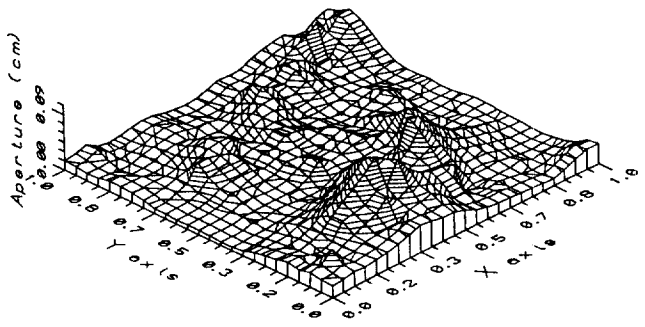

(a) Test No. 1: $\sigma=0.6$, $\lambda=0.5$, $R_o=1$

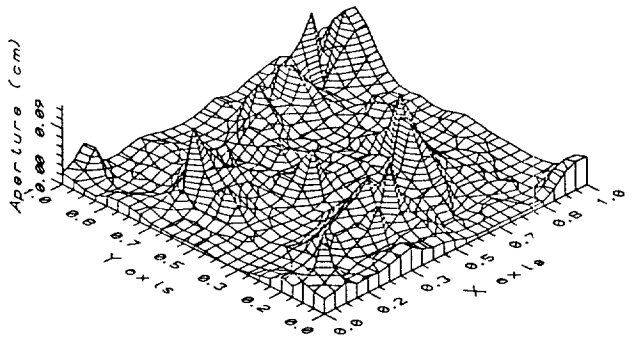

(b) Test No. 2: $\sigma=0.6$, $\lambda=0.1$, $R_o=1$

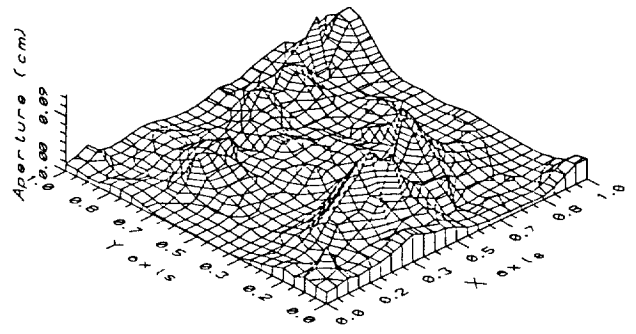

(c) Test No. 3: $\sigma=0.6$, $\lambda=0.25$, $R_o=1$

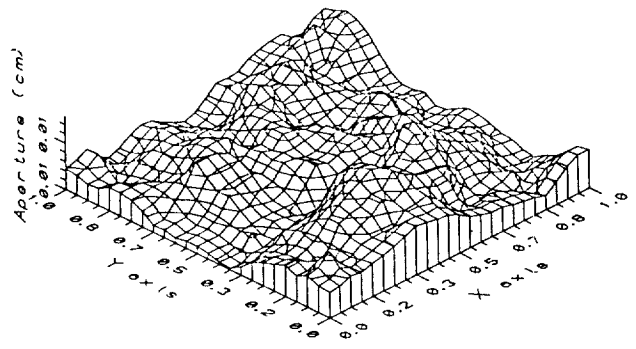

(d) Test No. 4: $\sigma=0.1$, $\lambda=0.5$, $R_o=1$

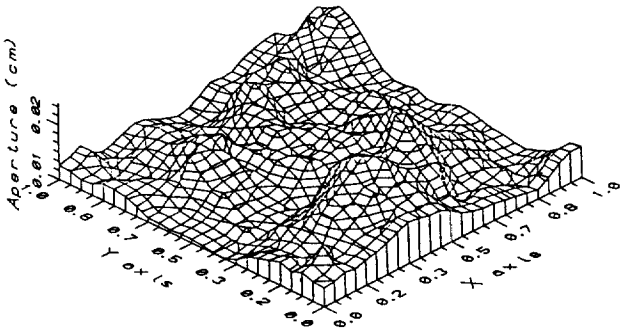

(e) Test No. 5: $\sigma=0.3$, $\lambda=0.5$, $R_o=1$

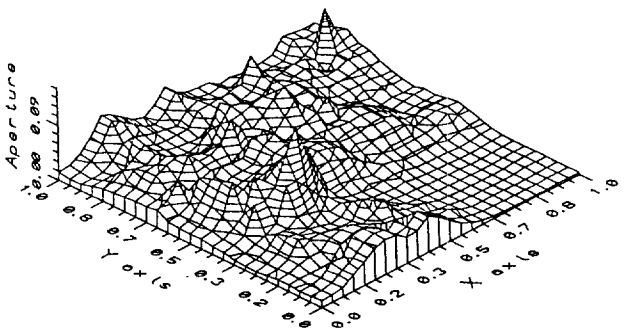

(f) Test No. 6: $\sigma=0.6$, $\lambda=0.5$, $R_o=2$

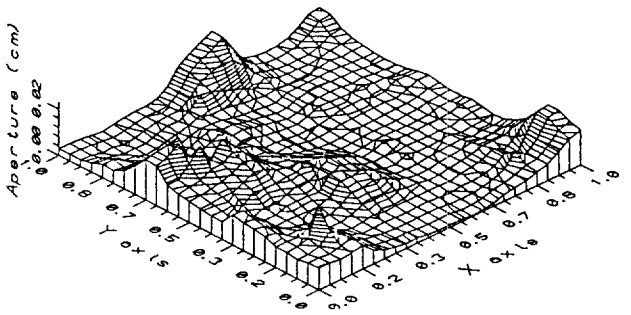

(g) Test No. 7: $\sigma=0.6$, $\lambda=0.5$, $R_o=3$

Fig. 2. Surface plot of aperture distribution.

constant injection/withdrawal rate as well as for a constant pressure condition. For a steady-state laminar flow, the volumetric flow rate through a parallel fracture may be written [Park et al., 1995]:

$$Q=\frac{1}{12\mu}\frac{b^3W}{L}\Delta P \tag{7}$$

where μ is the viscosity in g/cm-s, b is the aperture in cm, and

Table 2. Basic data used for the simulation

Symbol	Entity	Value	
L, W	length, width	100, 100	cm
Q	flow rate	3	ml/h
μ	viscosity of the fluid	0.01	g/cm-s
P_{out}	pressure at the outlet	1,013,333	dynes/cm^2
(X, Y)	inlet position	(0.71, 0.79)	
(X, Y)	outlet position	(0.11, 0.11)	
V	volume of the tracer solution	10	ml

ΔP is the pressure drop over L and W, length and width of the fracture plane, respectively. Eq. (7) may be applied to each of the subsquares enclosed by the grid lines. When the volumetric flow rate from node i to node j is Q_{ij}, the pressure drop from node i to node j can be written as

$$\Delta P = P_i - P_j = \frac{Q_{ij}}{\frac{2b_i^3\Delta y}{12\mu\Delta x}} + \frac{Q_{ij}}{\frac{2b_j^3\Delta y}{12\mu\Delta x}} = Q_{ij}\left[6\mu\frac{\Delta x}{\Delta y}\left(\frac{1}{b_i^3}+\frac{1}{b_j^3}\right)\right] \quad (8)$$

where P_i is the pressure at node i in dynes/cm^2, Δx and Δy are the length of x and y coordinate in a subsquare, respectively. Node i implies an index of the i-th subsquare in the fracture surface. Then the volumetric flow rate can be rewritten as

$$Q_{ij} = C_{ij}(P_i - P_j) \quad (9)$$

where C_{ij} is the flow conductance between nodes i and j in cm^{2}s/g and given by

$$C_{ij} = \frac{1}{6\mu}\frac{\Delta y}{\Delta x}\left(\frac{1}{b_i^3}+\frac{1}{b_j^3}\right)^{-1} \quad (10)$$

The mass balance at each node i may be written as

$$\sum_j Q_{ij} = \sum_j C_{ij}(P_i - P_j) = E_i \quad (11)$$

where E_i is the injection rate or withdrawal rate at node i. At the inlet and outlet the values of E_i are both set at 3 ml/hr. The symbol j stands for the four facing nodes of surrounding subsquares to node i. By rearranging Eq. (11) for every node, we obtain a system of linear equations in the form

$$[B]\ [P] = [C] \quad (12)$$

where [B] is a coefficient matrix of 400×400 elements describing flow conductance. The matrix [P] is an array of 400 elements describing pressure distribution and [C] is an array of 400 elements describing net flow rates. Except for the nodes at the inlet and outlet, the pressure at each node is an unknown to be solved with an iterative numerical method.

To simulate a real flow system, we adopt experimental system of Park et al.'s [1995]. They carried out a contaminant migration experiment with about 1×1 m scale granite block. The block had a natural fracture running parallel to the horizontal direction. The fracture did not have a constant aperture but had vaying aperture sizes between 0.1 mm and 1 mm. Tracers were injected as a point source at the certain borehole (0.71, 0.79), migrated in the fracture plane, and finally eluted at the withdrawal borehole (0.11, 0.11). Data of the experimental conditions are listed in Table 2. We also selected the same (X, Y) coordinates of the inlet and outlet as Park et al.'s setup. The simulated pressure field for Test No. 1 is shown in Fig. 3. The pressure drop between the injection and withdrawal points is about 26 dynes/cm^2 and the pressure at the outlet is almost the atmospheric pressure. The flow between adjacent nodes can be calculated using Eq. (9). After obtaining flow vectors at all the nodes, solute transport can be simulated in this flow field.

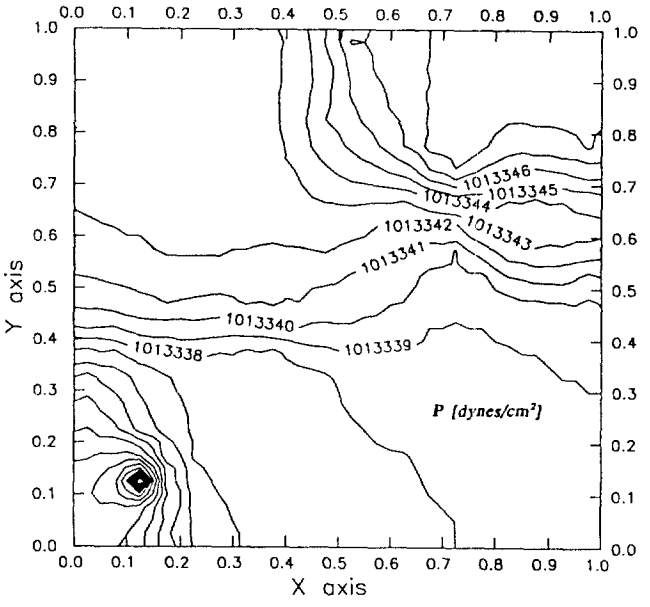

Fig. 3. Pressure distribution in the fracture of Test No. 1.

PARTICLE TRACKING METHOD FOR CONTAMINANT TRANSPORT

Contaminant transport in the fracture is investigated by tracking particles advected through the fracture. A particle, which is representing the mass of a contaminant contained in a defined volume of fluid, moves through a fracture with two types of motion. One motion is with the mean flow along stream lines and the other is random motion, governed by scaled probability. The particle tracking method similar to those used by Yamashita and Kimura [1990] and Desbarats [1990] is used.

At the injection point, a certain number of particles are introduced and distributed at each node between flow channels with a probability proportional to the flow rates. Particles are then convected by discrete steps from node to node until they reach the outlet node at which point the arrival time is recorded. Particle movement is regulated by the following algorithm.

1. At the injection point, a certain number of particles are introduced.
2. At a given node, calculate the volumetric flux across each four faces of the surrounding grid cell using Eq. (9).
   Q_{ij} (j=1, 2, 3, & 4)
3. Calculate the total outflow from the subsquare.
   $Q_i' = \sum_{j=1}^{4} Q_{ij}$
4. Assign the probability to each of the four possible flow directions. For inflow direction the probability is zero. For outflow direction the probability equal to the fraction of the total outflow

from the subsquare.

$$p_{ij}=Q_{ij}/\sum_{j=1}^{4} Q_{ij}$$

5. Generate random number and choose an outflow direction according to the discrete probability distribution.

6. Move particle to the next node in the selected direction at a velocity equal to the total outflow rate from the subsquare. This ensures conservation of total mass flux through the cell at any given particle step and, over many passages, conservation of mass flux in each direction.

7. Increment the cummulative travel time by an appropriate amount.

$$t_{cum}=\sum_{i=1}^{n} t_i$$

8. Repeat from step 2 until the particle arrives at the outlet.

9. Repeat from step 1 for the number of particles.

10. Sum up the results.

Preliminary calculations have been carried out for a total number of input particles ranging from several hundreds to 10^6 in order to investigate the effect of the number of particles on the elution profile because the numerical accuracy is considered to be dependent on the number of particles used. As expected, the calculation using larger number of particles gives the better approximation. However, there is no significant improvement in the numerical results when the total number of particles is larger than 10^5. Calculations using more than 5,000 particles are adequate since they yield stable elution curves that have few spurious artifacts due to the finite number of particles employed. Thus 10,000 particles are chosen in this study. The residence time for conservative contaminant in a given subsquare is determined from the total flow through the subsquare and its volume. The residence time of a particle along each path was obtained as the sum of the residence times at all subsquares through which the particle had passed. Particles are let in at the injection point (0.71, 0.79) and collected at the withdrawal point (0.11, 0.11), those are arbitrarily chosen but from a real fracture system as shown in Table 2. A plot of the number of particles collected at the outlet at different arrival times constitutes the elution profile. When the number of particles in each cell at a certain time is counted, it shows a migration plume.

HYDRODYNAMIC PARAMETERS

The transport properties for the different realizations are studied by comparing the mean residence time and the hydrodynamic dispersion. The mean residence time and variance may be used to determine the Peclet number Pe, which is a dimensionless measure of the hydrodynamic dispersivity σ_t [Levenspiel, 1972]:

$$\frac{2}{P_e}=\frac{\sigma_t^2}{t_m^2} \tag{13}$$

where t_m is the mean residence time,

$$t_m=\frac{\int_0^\infty t\,C\,dt}{\int_0^\infty C\,dt} \tag{14}$$

and σ_t^2 is the second moment as a measure of hydrodynamic dispersivity.

$$\sigma_t^2=\frac{\int_0^\infty (t-t_m)^2 C\,dt}{\int_0^\infty C\,dt} \tag{15}$$

Here C(t) is the concentration at time t. If an ideal pulse is imposed, then the normalized concentration C_θ is

$$C_\theta=\frac{2}{2\sqrt{\pi/P_e}}\exp\left[\frac{-P_e(1-\theta)^2}{4}\right] \tag{16}$$

and

$$C_{\theta max}^2=\frac{P_e}{4\pi} \tag{17}$$

where θ is the normalized time, $\theta=t/t_m$. Even though the test cases are not ideal flow systems, we can get some useful informations by comparing hydrodynamic parameters for each test case.

MIGRATION PLUMES AND ELUTION PROFILES

Fig. 4 shows the spatial distribution of particles for Test No. 1 at times from 5 hours to 40 hours after injection. It is a contour plot of the number of particles in the fracture surface. The number of particles at each point is normalized by dividing with the total number of particles input and it stands normalized concentration of the migration plume. Thus the numerical values in the contour maps mean the normalized concentration, C/Co, in which Co is the initial input concentration. These plots show that the contaminant moves as a broad delta shape rather than moving a straght line from the inlet to the outlet. Comparing to the aperture distribution as shown in Figs. 1 and 2(a), the migration plume displays the preferred path of large volumetric flow rate that is formed because of the variation of the apertures within the fracture plane. In other words, flow through the fracture seeks out the least resistive pathways composed of largest apertures. Flow in small aperture will be little because the local resistance is inversely proportional to the cube of local aperture. When the real fracture system [Park et al., 1995] was opened after migration test, the trace of migration showed same trend of tortuous flow with the simulated one.

The elution curves involve the residence times of all possible flow paths which originate from the injection point and terminate on the exit point. Here t_m is calculated by taking the average of all the residence times of the 10,000 particles. In Fig. 5, the elution profiles of contaminant transport in two dimensions through these variable apertures show a fast rise at early times, since the majority of particles take the fast flow paths, then show a long tail in the elution curve due to a small fraction of particle meandering through the fracture of very small volumetric flow rates. The elution curves show the presence of a multipeak, suggesting that some channeling take place in the fracture. The elution curve of the real system also showed the same trend with the simulated one even though they did not agree with each other exactly in the morphology of the fracture plane. Therefore, stochastic generation method can describe the migration characteristics in the fracture successfully.

PARAMETER SENSITIVITY STUDIES

The parameter sensitivity of the aperture function is studied

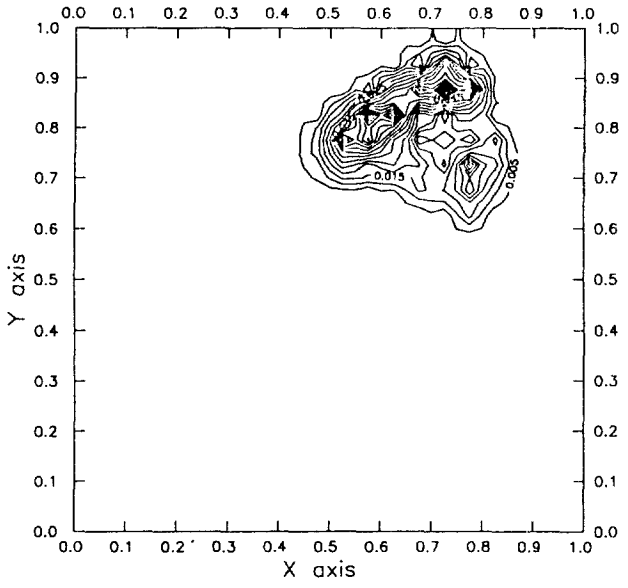

(a) after 5 hours

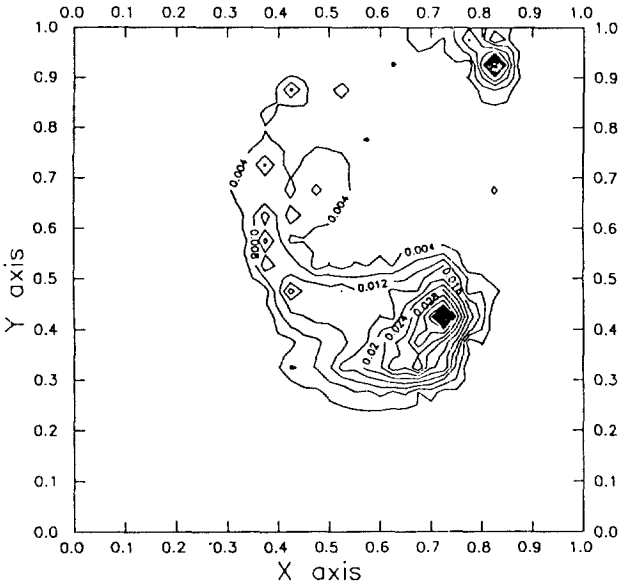

(c) after 20 hours

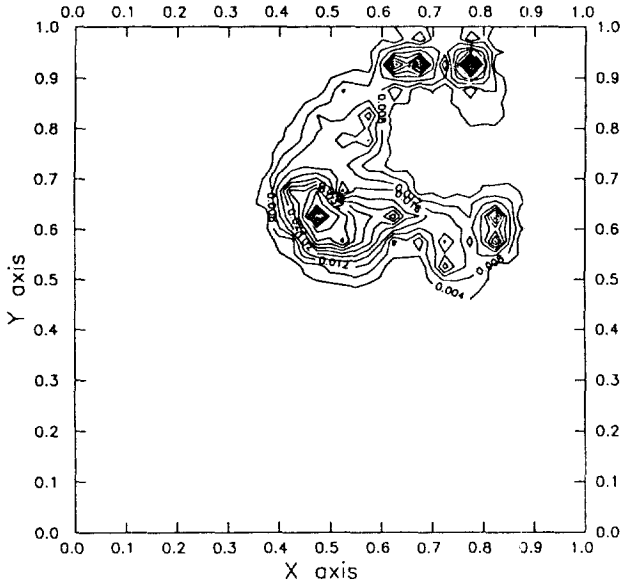

(b) after 10 hours

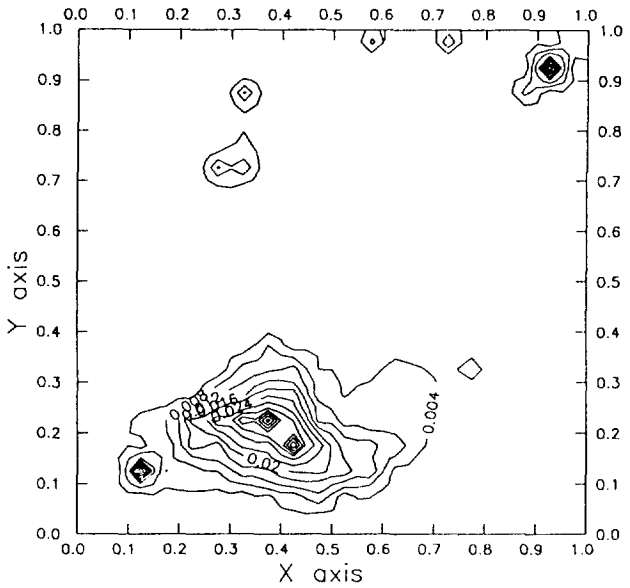

(d) after 40 hours

Fig. 4. Migration plume of Test No. 1.

by simulating the fluid flow and contaminant transport with varying the aperture characteristics. The introduced properties are (1) the standard deviation in the lognormal aperture density distribution, σ, (2) the spatial correlation length of the apertures λ, and (3) different realizations of the aperture field of the same geometric parameters with different initial numbers, R_0. The fracture volume is kept constant in all simulations by setting the value of the mean aperture 0.1 mm. Seven realizations of aperture field from Test No. 1 to No. 7 corresponding to each set of parameters are generated in order to study the dependence of parameters. The flow properties chosen as criteria to compare the different cases are the mean fracture residence time t_m and the Peclet number Pe or hydrodynamic dispersivity σ_l. They are grouped under the three sets of aperture parameters (λ, σ, R_0) and are arranged in Table 1. Pe is calculated with Eq. (17) from the elution curve. σ_l is calculated by two ways: using the particle tracking data with Eq. (15) and using the elution curve with Eq. (13). The values of σ_l calculated by these ways agree with each other except for the high dispersion cases. In case of high hydrodynamic dispersion such as Test No. 2, σ_l^2 is strongly influenced by the tail of the elution curve and the determination of Peclet number by means of Eq. (13) yields values dominated by the tail. Thus in order to ignore the extreme tailing effect we do not take into account the tailing part of the elution curve after that 90% of the particles are eluted. Moreover we are not focusing on getting an absolute value of Pe or σ_l but relative importance among parameters. Thus comparing relative ratios of the parameter values is more meaningful. Calculated values of t_m, Pe and σ_l for the seven test cases are arranged in Table 1 and their results are analyzed in the following section.

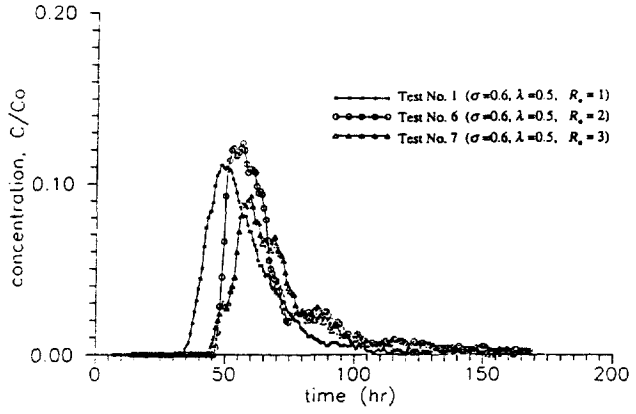

Fig. 5. Elution curves for different realization with different initial numbers.

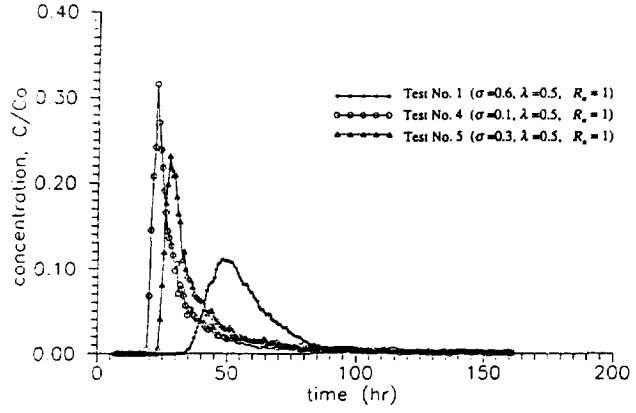

Fig. 6. Elution curves for various σ values, σ=0.1, 0.3, and 0.6.

1. Dependence on Different Realizations

Set 1 deals with three realizations of statistically generated apertures with the identical lognormal aperture density distribution but with different random number seeds: the mean $\nu=1.0$, the standard deviation $\sigma=0.6$, the correlation length $\lambda=0.5$ and the random number seeds $R_s=1$, 2, and 3. Three different aperture fields are shown in Figs. 2(a), 2(f) and 2(g). The morphology of the fracture surface and flow paths are changed from realization to realization. Thus the elution curve may also be changed according to the change of flow paths. However values of t_m, σ_t, or Pe as well as elution curves do not change significantly comparing to other cases as shown in Table 1. That is, when the geostatistical relationship is maintained in each realization, the overall flow resistance does not change significantly and elution curves also show a similar trend. Therefore the most important variation between the different realizations within the same set of aperture parameters was observed in the flow path through the fracture.

2. Dependence on Aperture Variance

Set 2 deals with the effect of aperture variation while the correlation length and the mean of aperture are kept constant. Also the overall morphology of surface and flow path are schemed to be roughly maintained with σ variation while the aperture and the flow resistance are changed at each point in the fracture as shown in Figs. 2(a), 2(d) and 2(e). Fig. 7 shows the elution curves for these σ values. For a larger σ the mean residence time t_m is bigger. These trends may be explained by the fact that a larger

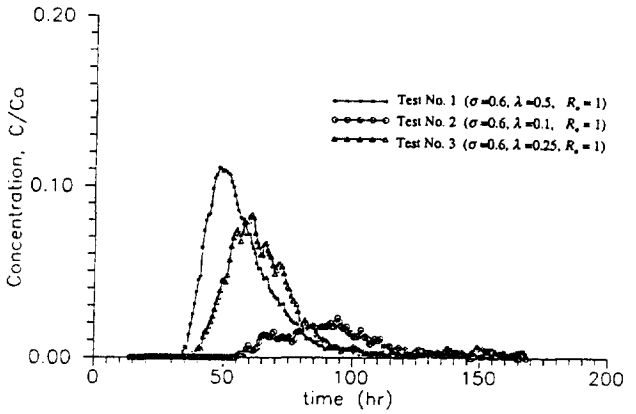

Fig. 7. Elution curves for various λ values, λ=0.1, 0.25, and 0.5.

σ means a greater number of small apertures. The flow resistance is greatly increased in the small apertures. On the other hand, the large apertures increase the flow in the fracture only if they are interconnected directly along the flow path. Otherwise, they may increase the residence time in the fracture but not the flow rate in it. The hydrodynamic dispersion of the tracer transport is increased when σ increases. The σ_t^2 is about 5.71 for $\sigma=0.6$, while σ_t^2 is 0.77 for $\sigma=0.1$. This shows the strong influence of the width of the fracture aperture distribution on the hydrodynamic dispersion of contaminants flowing through it. In this model, we assumed that the dispersion was due mainly to channeling effects. This means that for a very small σ the hydrodynamic dispersion is negligible. In the limit when σ is zero, the σ_t may be zero, i.e., plug flow in a parallel plate fracture having constant aperture.

3. Dependence on Correlation Length

Set 3 deals with the effect of correlation length. As the case of σ variation, the overall morphology of surface and flowpaths are schemed to be roughly maintained with λ variation even though the value of aperture and the flow resistance are changed at each point in the fracture surface as shown in Figs. 2(a), 2(b) and 2(c). The simulated results in Fig. 7 and Table 1 show that the hydrodynamic properties in the fracture (σ_t, t_m) are sensitive to the values of λ. The hydrodynamic dispersion of the tracer in the fracture is increased from 2.7 to 200, i.e., the Peclet number is decreased from 0.35 to 0.01, when λ is decreased from 0.5 to 0.1. The use of smaller value of λ yields larger hydrodynamic dispersion, that is, a fracture with a network of many interconnected channels. This trend is shown clearly in Fig. 7. As the value of λ decreases, multipeak is observed distinctively. If the value of λ is small enough, then the porous medium model can be applied.

SUMMARY AND CONCLUSIONS

Simulated migration plumes and elution profiles show that a broad distribution of apertures in the fracture develops the flow channeling phenomena. In this aspect, the variable aperture character of a two dimensional fracture causes its fluid flow and contaminant transport properties to be quite different from those derived from the parallel-plate model of the fracture. For contaminant transport, the channeling implies that some fast pathways might transport the majority of the contaminants while a small portion of contaminants meandering through the fracture gives

rise to as long tail. Results of the parameter sensitivity studies show that the most important parameter which affects flow and tracer transport is the correlation length. If the correlation length is increased, the flow residence time and the hydrodynamic dispersion are decreased. Thus, if the correlation length is very small, the porous medium model may be applied. The standard deviation in the lognormal aperture distribution plays a secondary role in influencing the flow and tracer transport in the fracture. When the relationship of geometric parameters are maintained, the change of flow paths does not give significant effect on the elution profile.

NOMENCLATURE

A : covariance matrix
b_i : aperture in node i [cm]
C : concentration of the contaminant [g/ml]
C_{ij} : flow conductance between node i to node j
E[ ]: expectation operator
E_i : injection rate or withdrawal rate at node i [ml/hr]
M : lower-triangular matrix of matrix A
Pe : Peclet number, $Pe=u\lambda/D_L$
P_i : pressure at node i [dyne/cm^2]
p_{ij} : probability of flow direction from node i to node j
Q_{ij} : volumetric flow rate between node i to node j [cm^3/s]
r : distance between any two points in the fracture plane [cm]
R_0 : initial number to generate a random number set
t_m : mean residence time [hr]
Y : distribution of the aperture

Greek Letters

α : autocorrelation parameter
ε : vector, each element has a value between 0 and 1
λ : correlation length
μ : fluid viscosity [g/cm-s]
ν : mean of aperture distribution [cm]
θ : dimensionless elution time, $\theta=t/t_m$
σ^2 : variance of aperture distribution
σ_l : hydrodynamic dispersion

REFERENCES

Bianchi, L. and Snow, D., "Permeability Crystalline Rock Interpretated from Measured Orientations and Apertures fo Fractures", *Annu. Arid Zone*, **8**, 231 (1968).

Choi, H. J., Lee, H. S. and Han, K. W., "A Theoretical Study on the Migration of Radionuclides in a Radwaste Disposal System", *HWAHAK KONGHAK*, **26**, 229 (1988).

Desbarats, A. J., "Macrodispersion in Sand-Shale Sequences", *Water Resour. Res.*, **26**, 153 (1990).

El-Kadi, A. I., "Model Variability in Groundwater Flow", International Groundwater Modeling Center, GWMI 84-10, Holcomb Research Institute, Butler Univ. (1984).

Keum, D. K., Cho, W. J., Hahn, P. S. and Park, H. H., "Study on the Radionuclide Migration Modeling for a Single Fracture In Geologic Media", *J. of Kor. Nucl. Soc.*, **26**, 401 (1994).

Lee, Y. M., Cho, W. J., Han, K. W. and Park, H. H., "Verification of a Nuclide Migration Model by Comparing with Other Models", *J. of the Kor. Nucl. Soc.*, **22**, 304 (1990).

Levenspiel, O., Chemical Reaction Engineering, 2nd ed., John Wiley, New York (1972).

Mantoglou, A. and Wilson, J. L., "The Turning Band Method for Simulation of Random Fields Using Line Generation by a Spectral Method", *Water Resour. Res.*, **18**, 1379 (1982).

Moreno, L., Neretnieks, I. and Eriksen, T., "Analysis of Some Laboratory Tracer Runs in Natural Fissures", *Water Resour. Res.*, **21**, 951 (1985).

Moreno, L. and Neretnieks, I., "Flow and Nuclide Transport in Fractured Media", *J. of Contaminant Hydrology*, **14**, 163 (1993).

Moreno, L., Tsang, C. F., Hale, F. V. and Neretnieks, I., "Flow and Tracer Transport in a Single Fracure", *Water Resour. Res.*, **24**, 2033 (1988).

Nash, J. C., "Compact Numerical Methods for Computers: Linear Algebra and Function Minimization", John Wiley and Sons, New York (1979).

Neretnieks, I., Eriksen, T. and Tahtinen, T., "Tracer Movement in a Single Fissure in Granitic Rock", *Water Resour. Res.*, **18**, 849 (1982).

Park, C. K., Vandergraaf, T. T., Drew, D. T. and Hahn, P. S., "Interpretation of Migration of Radionuclides in a Rock Fracture Using a Particle Tracking Method", *J. of Korean Nucl. Soc.*, **27**, 176 (1995).

Smith, L. and Schwartz, F. W., "Mass Transport 1, A Stochastic Analysis of Macroscopic Dispersion", *Water Resour. Res.*, **16**, 303 (1980).

Tang, D. H., Frind, E. O. and Sudicky, E. A., "Contaminant Transport in Fractured Porous Media", *Water Resour. Res.*, **17**, 555 (1981).

Tsang, Y. W. and Tsang, C. F., "Channels Model of Flow through Fractured Media", *Water Resour. Res.*, **23**, 467 (1987).

Tsang, Y. W., Tsang, C. F., Neretnieks, I. and Moreno, L., "Flow and Tracer Transport in Fracture Media-A Variable Aperture Channel Model and its Properties", *Water Resour. Res.*, **24**, 2049 (1988).

Vandergraaf, T. T., Park, C. K. and Drew, D. J., "Migration of Conservative and Poorly Sorbing Tracers in Granite Fractures", Proceedings of 5th International High Level Radioactve Waste Management, Las Vegas (1994).

Yamashita, R. and Kimura, H., "Particle Tracking Technique for Nuclide Decay Chain Transport in Fractured Porous Media", *J. of Nuclear Sci. and Tech.*, **27**, 1041 (1990).